

Contents lists available at ScienceDirect

Combustion and Flame

journal homepage: www.sciencedirect.com/journal/combustion-and-flame





Ignition enhancement and NO_x formation of NH_3 /air mixtures by non-equilibrium plasma discharge

Xingqian Mao^{1,*}, Hongtao Zhong¹, Ning Liu, Ziyu Wang, Yiguang Ju

Department of Mechanical and Aerospace Engineering, Princeton University, Princeton, NJ 08544, USA

ARTICLE INFO

Keywords: Plasma assisted ignition Non-equilibrium excitation Ammonia Ignition enhancement NO₂ formation

ABSTRACT

This work computationally studies plasma assisted low temperature NH₃/air ignition and NO_x formation in a repetitively-pulsed nanosecond discharge at atmospheric pressure by using an experimentally-validated plasmacombustion kinetic model. The results show that plasma discharge significantly enhances low temperature NH₃ ignition. Compared with thermal ignition, the ignition delay time is shortened by 2-5 orders of magnitude due to the kinetic enhancement of excited species and radicals. The radicals (NH2, NH, H and O) produced through electron impact dissociation and quenching of electronically excited N2*, O(1D) and N(2D) promote OH production and further accelerate NH3 oxidation. The results show that there exists a non-monotonic dependence of ignition delay time on the reduced electric field strength. The optimum ignition enhancement is achieved at 250 Td at which the production of electronically excited species and radicals is most efficient. The vibrationally excited species produced at lower electric fields (<100 Td) are less effective in enhancing ignition because they only induce gas heating through the fast vibrational-translational relaxation by NH₃ and H₂O. At a higher electric field, although the efficient production of NH2, NH, H, O and OH by plasma creates new low temperature reaction pathways in enhancing low temperature NH $_3$ ignition, the ignition is inhibited through NH + NO = N_2O + H and chain-termination reaction $NH_2 + HO_2 = NH_3 + O_2$. The ignition delay times at different equivalence ratios show that the ignition enhancement by plasma is more effective at fuel-lean conditions due to the faster generation of $N_2(B)$, $O(^1D)$ and O from air, leading to accelerated N_3 oxidation via $O(^1D) + NH_3 \rightarrow NH_2 + OH$, $NH_3 + O = NH_2 + OH$ and $NH_2 + O = NH + OH$. The sensitivity analysis shows that the reactions involving O and O(¹D) production are more effective on NH₃ ignition enhancement than the fuel dissociation by electrons. Moreover, the ignition is also enhanced by NO_x formation in plasma via reactions $NH_2 + NO = NNH + OH$ and $NO + HO_2 = NO_2 + OH$. This work advances the understanding of non-equilibrium excitation and NO_x formation by plasma discharge on low temperature NH3 ignition.

1. Introduction

To address the key challenges for carbon neutrality, such as energy sustainability, energy security, and climate change, renewable fuels play an increasingly important role in recent years. As one of the promising renewable fuels and a hydrogen carrier, ammonia (NH₃) draws great attention [1,2]. NH₃ is identified as zero-carbon and sustainable alternative to conventional hydrocarbon fuels. Compared with hydrogen, NH₃ has the advantages of higher volumetric energy density and lower cost per unit stored energy for safe storage and transportation [1,2]. It can be applied to internal combustion engines (ICE) [3], gas turbines [4] and propulsion systems [5]. The utilization of NH₃ provides a new

method towards carbon-neutral future.

However, the NH_3 combustion still faces many challenges [1,2]. For example, NH_3 has poor combustion properties such as low specific energy, slow laminar burning velocity, and narrow flammability range. In addition, NH_3 combustion has high NO_x emissions. These critical problems need to be solved by developing efficient NH_3 combustion technologies.

In the past decades, non-equilibrium plasma has shown remarkable advantages in enhancing ignition, extending flammability, accelerating low temperature oxidation, and reducing emissions [6–12]. Volumetric production of chemically active species, fuel fragments and gas heating in a plasma discharge can modify conventional combustion pathways

^{*} Corresponding author.

E-mail address: xingqian@princeton.edu (X. Mao).

¹ These authors contributed equally to this work.

and accelerate fuel oxidation via kinetic, thermal and transport enhancement pathways [6,7]. Therefore, plasma assisted combustion provides a new method for the application of NH₃ in combustion. Several works [13-21] have discussed the effects of non-equilibrium plasma on NH₃ combustion both by experimental [13-16] and numerical approaches [17-21]. The effects of non-equilibrium plasma on NH₃/air combustion have been studied experimentally in swirl flames [13–16]. The results showed that plasma simultaneously extended the lean blowoff limits of NH3 flames [13-16] and reduced NOx emission [13,16]. To understand the kinetic enhancement by plasma, numerical modeling has been conducted in plasma assisted NH3 combustion [17-21]. Faingold et al. [18] and Taneja et al. [20] investigated the ignition characteristics of NH3 mixtures in a nanosecond repetitively pulsed discharge. Shahsavari et al. [21] studied the effects of plasma pulse and mixture properties on NH3 combustion. The results showed that the excited species and radicals generated by plasma significantly extended NH₃ ignition limits. These studies advanced the understanding of kinetic enhancement by plasma discharge on NH3 combustion. However, due to the lack of validated plasma assisted NH₃/O₂/N₂ combustion kinetic model, the plasma reaction pathways on ignition enhancement at low temperatures are still not-well understood. Some of the results are even contradictory. For example, Taneja et al. [20] studied that the vibrational-translational (VT) relaxation of vibrationally excited $NH_3(\nu = 2)$ increased the mixture reactivity at a moderate reduced electric field E/N (electric field strength/gas number density) of 150 Td. This resulted in shorter ignition delay time compared with the condition at 550 Td. However, the results by Shahsavari et al. [21] were completely opposite which the shorter ignition delay time was achieved at 550 Td. Meanwhile, the dissociation of NH₃ by electronically excited N₂* and N(²D) was not considered in these works. Therefore, many open questions such as the roles of vibrationally excited species, electronically excited species, and the effects of NOx formation on NH3 ignition remain.

Recently, Zhong et al. [22] developed a NH₃/O₂/N₂ plasma-combustion kinetic model based on in-situ laser diagnostics. Important species including NH3, NO, NO2, N2O, H2O and OH were measured and the non-equilibrium N2O/NOx chemistry in plasma assisted low temperature NH₃ oxidation was studied and validated. This provides an opportunity to further study the plasma assisted low temperature NH3 ignition by numerical modeling using the experimentally-validated kinetic model. Motivated by the discussion above, in this work, the ignition enhancement of NH₃/air in a repetitively-pulsed nanosecond discharge (NSD) is studied. First, the effects of non-equilibrium excitation at different reduced electric fields on low temperature NH3 ignition are studied. Then, the key species and reaction pathways on ignition enhancement are investigated. After that, the ignition by non-equilibrium plasma at different equivalence ratios is studied. Finally, the effects of NO_x formation on ignition enhancement are further discussed.

2. Numerical methods and model validation

2.1. Numerical method and kinetic model

The numerical modeling for the time evolutions of species densities and temperature in a plasma assisted NH₃/air ignition system is conducted by an integrated zero-dimensional (0-D) hybrid ZDPlasKin-CHEMKIN model [23–25]. The model incorporates the plasma kinetics solver ZDPlasKin [26] and the combustion kinetics solver CHEMKIN II [27] by a time-splitting scheme. The electron impact reaction rate constants and transport parameters are solved by the Boltzmann equation solver BOLSIG+ [28] incorporated in ZDPlasKin. The detailed governing equations and validations of hybrid ZDPlasKin-CHEMKIN model have been described in detail in previous studies [23,24].

An experimentally validated plasma-combustion kinetic model of $NH_3/O_2/N_2$ [22] recently developed at Princeton is used in this work.

The kinetic model incorporates a plasma kinetic sub-model and a combustion kinetic sub-model. There are 77 species in the kinetic model, 894 reactions in the plasma kinetic sub-model and 230 reactions in the combustion kinetic sub-model. The vibrationally excited species NH₃(v = 2) (0.118 eV), NH₃(ν = 4) (0.202 eV), NH₃(ν = 1,3) (0.42 eV), O₂(ν = 1)- $O_2(v = 4)$ (0.193-0.772 eV), $N_2(v = 1)$ - $N_2(v = 8)$ (0.29-2.35 eV); electronically excited species $O_2(a^1\Delta_g)$, $O_2(b^1\Sigma_g^+)$, O_2^* , $O(^1D)$, $O(^1S)$, N₂* (N₂(A), N₂(B), N₂(a'), N₂(C)), N(²D); ions NH⁺, NH₂⁺, NH₃⁺, NH₄⁺, N_2H^+ , O_2^+ , O_4^+ , N_2^+ , N_4^+ , H_2^+ , H_3^+ , H_2O^+ , H_3O^+ , O^- , O_2^- , O_4^- , OH^- ; and electrons are included in the kinetic model. The rotationally excited species O₂(rot) and N₂(rot) are considered to provide gas heating by fast rotational-translational (RT) relaxation within 0.5 ns [8]. The plasma sub-model incorporates the reactions of electron impact vibrational and electronic excitation, dissociation, ionization and attachment, and electron detachment, as well as quenching of vibrationally and electronically excited species, charge exchange, ion-ion and electron-ion recombination. The VT relaxation, vibrational-vibrational (VV) exchange and chemical reactions by vibrationally excited species are included. The electron impact cross section data are obtained from the online database LXCat [29]. The cross sections data of NH₃ are originally from the Hayashi database [30]. The cross sections of O2, N2 and H2O come from the Biagi [31], Phelps [32] and Morgan [33] database, respectively. The reactions between electron and intermediate species are not considered due to their low concentrations. For the combustion sub-model, a detailed NH₃/O₂/N₂ combustion model from Thorsen et al. [34] with an O₃ sub-model [35] is used. The reaction rate constants with large uncertainties at low temperatures are updated based on the experimental data, which can be found in [22] and the supplementary materials.

2.2. Model validation

To validate the $NH_3/O_2/N_2$ plasma-combustion kinetic model, a plasma assisted low temperature NH_3 oxidation experiment is conducted at room temperature and 30 Torr. The schematic of the experimental setup is shown and discussed in detail in [22,36,37]. A repetitively-pulsed nanosecond discharge is applied to a plane-to-plane dielectric barrier discharge (DBD) for plasma generation. The species (NH_3 , NO, NO_2 , N_2O , H_2O and OH) and temperature measurements are conducted by the *in-situ* mid-IR tunable diode laser absorption spectroscopy (TDLAS) [38,39].

Fig. 1 shows the comparison of H₂O, N₂O and NO concentrations between experimental measurements and model predictions in a fuel rich 0.110 NH₃/0.055 O₂/0.835 N₂ ($\varphi=1.5$) mixture with a continuous

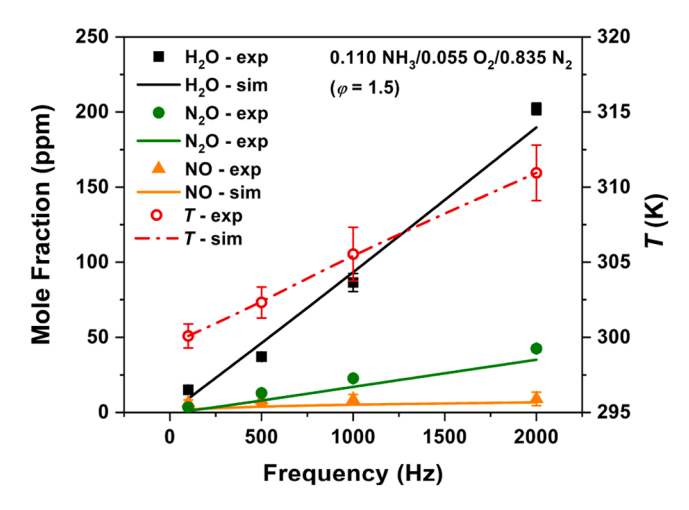


Fig. 1. Comparison of species concentrations between experimental measurements and model predictions in a $0.110 \, \text{NH}_3/0.055 \, \text{O}_2/0.835 \, \text{N}_2$ mixture with a continuous discharge at $100\text{-}2000 \, \text{Hz}$.

discharge at 100-2000 Hz. The deposited energy from the time-dependent results [22], as well as the measured temperature and voltage are used as inputs for all numerical modeling. The residence time at 298 K is ~ 0.136 s. With the increase of temperature at higher frequencies, the residence time decreases correspondingly. The results show that the species concentrations increase with pulse repetition rate. More discharge energy applied with higher frequencies leads to faster NH $_3$ oxidation at low temperatures. The good agreement validates the plasma-combustion kinetic model and the numerical methods. This kinetic model is also validated for fuel lean NH $_3/O_2/N_2$ ($\varphi=0.8$) and NH $_3/O_2$ ($\varphi=0.07$) mixtures [22].

3. Results and discussion

3.1. Effects of non-equilibrium excitation on low temperature NH_3 ignition

To study the non-equilibrium excitation effects of plasma on low temperature NH $_3$ ignition, it is critical to understand the processes of electron energy transfer and the production of chemically active species in a plasma discharge. Fig. 2 shows the fractions of electron energy deposition into different excitation modes in a stochiometric NH $_3$ /air (0.219 NH $_3$ /0.164 O $_2$ /0.617 N $_2$) mixture as function of E/N calculated by BOLSIG+ [28]. Below 10 Td, electron energy is primarily deposited into the rotational excitation mode and the vibrational excitation of NH $_3$ (ν). With the increase of E/N, more discharge energy goes to N $_2$ (ν) between 10 and 100 Td. Meanwhile, the energy deposition in the dissociation of NH $_3$ and O $_2$ as well as the electronic excitation of N $_2$, and the dissociation and ionization of NH $_3$, O $_2$ and N $_2$ dominate the discharge energy transfer.

The modeling of plasma assisted ignition is conducted in a stochiometric NH₃/air mixture at 300–1000 K and atmospheric pressure in an adiabatic system. A repetitively-pulsed nanosecond discharge with a pulse repetition rate of 30 kHz is applied. The discharge pulses are applied until the ignition occurs. For the comparison of ignition enhancement at different E/N values, the same discharge energy of 0.4 mJ/cm³ is applied in each pulse. The pulse width is adjusted to keep the energy deposition per pulse constant as the gas temperature and E/N change. The degree of ionization is below 10^{-5} in all conditions at which the super-elastic collisions and reactions between electron and intermediate species are less important. To compare with the NSD assisted ignition, the ignition delay times of thermal ignition and autoignition are calculated. Thermal ignition represents the ignition occurs when the

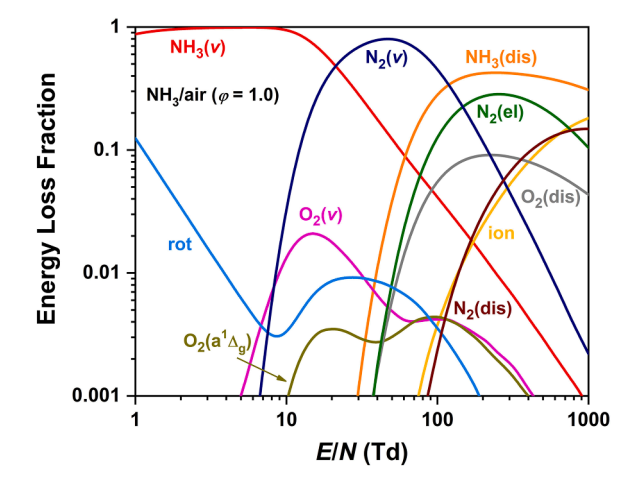


Fig. 2. Fractions of electron energy deposition into different excitation modes as a function of E/N in a stochiometric NH₃/air mixture. (rot: rotational excitation; ν : vibrational excitation; el: electronic excitation; dis: dissociation; ion: ionization).

same amount of discharge energy in the NSD assisted ignition condition is applied as a thermal contribution to increase the initial temperature. Autoignition refers to the ignition occurs without any plasma or thermal energy input at the given temperature. The ignition delay time is defined as the time interval between the starting point and the time of thermal runaway.

Fig. 3(a) shows the comparison of ignition delay time by autoignition, thermal ignition and NSD assisted ignition with different E/Nas a function of temperature (T). Compared with autoignition and thermal ignition, the results clearly show that the nanosecond discharge enhances ignition and shortens ignition delay time, especially at low temperatures. The maximum ignition enhancement is achieved at 250 Td with minimum discharge energy. This is attributed to the efficient production of electronically excited species (N_2 * and $O(^1D)$) and radicals by electron impact excitation and dissociation at 250 Td, as shown in Fig. 2. It can be seen that the autoignition is unlikely to occur below 1000 K due to the slow chain-initiation and chain-branching reactions for NH₃ oxidation at low temperature. For thermal ignition, the ignition delay time is 2-5 orders of magnitude higher compared with NSD assisted ignition above 400 K at 250 and 600 Td. At 300 K, even a significant amount of thermal energy is applied (see Fig. 3(b)), the ignition still fails at the thermal ignition case. This indicates the important role of kinetic enhancement on ignition by plasma discharge at low temperature. However, for NSD assisted ignition, the ignition enhancement at 50 Td is less efficient with even more energy input compared with the conditions at 250 and 600 Td, as shown in Fig. 3(b). This is because the vibrationally excited species are the major products at low E/N. They mainly provide thermal contribution via VT relaxation which are less efficient on ignition enhancement, which will be discussed in Section 3.2.

3.2. Key species and reaction pathways on ignition enhancement

Fig. 4 shows the time evolutions of chemically active species produced in the nanosecond discharge (grey region) and afterglow stage. The results show that all the excited species, radicals and electron increase exponentially via electron impact excitation, dissociation and ionization reactions during the nanosecond discharge. Among the excited species, Fig. 4(a) shows that the vibrationally excited species $NH_3(v = 2)$ and $N_2(v = 1)$ have the highest concentrations. In the afterglow stage, the concentration of $NH_3(v=2)$ decreases after 10 ns via VT relaxation reaction with NH₃ (R1). The mole fraction of vibrationally excited $N_2(\nu = 1)$ first increases at the timescale of nanosecond to tens of microseconds through VV exchange reaction (R2) and VT relaxation reaction (R3) from higher vibrational level $N_2(\nu = 2)$ - $N_2(\nu =$ 8). A similar increasing trend of $O_2(v = 1)$ is also observed in the afterglow stage. Fig. 4(a) shows that the vibrationally excited species $N_2(\nu = 1)$ and $O_2(\nu = 1)$ have long lifetimes. However, over 99% of them are quenched via VT relaxation with molecules such as NH3 and H2O through (R4) and (R5). Therefore, the vibrationally excited species only provide thermal contribution to ignition enhancement.

$$NH_3(v = 2) + NH_3 \rightarrow NH_3 + NH_3$$
 (R1)

$$N_2(v = n) + N_2 \rightarrow N_2(v = n-1) + N_2(v = 1) (n = 2-8)$$
 (R2)

$$N_2(v = 2) + NH_3 \rightarrow N_2(v = 1) + NH_3$$
 (R3)

$$N_2(v = 1) + NH_3/H_2O \rightarrow N_2 + NH_3/H_2O$$
 (R4)

$$O_2(v = 1) + NH_3/H_2O \rightarrow O_2 + NH_3/H_2O$$
 (R5)

For the electronically excited species N_2^* , $O(^1D)$ and $N(^2D)$, Fig. 4(a) shows that their concentrations decrease rapidly within 10 ns in the afterglow stage. The electrically excited N_2^* quenched via reactions (R6-R9) promotes the dissociation of NH_3 and O_2 as well as the production of NH_2 , NH, H, H_2 , O and $O(^1D)$. $O(^1D)$ and $O(^2D)$ are quenched by the reactions with $O(^2D)$ and $O(^2D)$ and $O(^2D)$ are quenched by $O(^2D)$ and $O(^2D)$ and $O(^2D)$ are quenched by $O(^2D)$ 0.

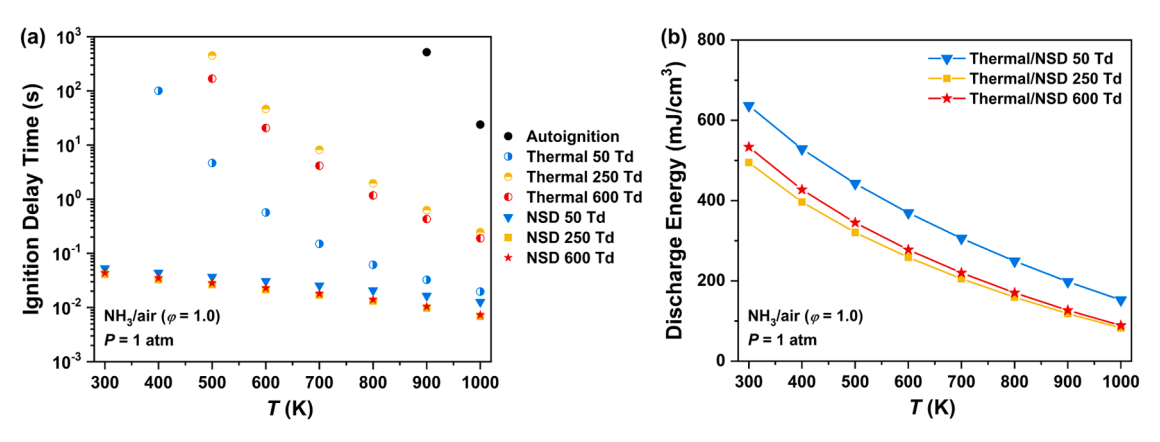


Fig. 3. (a) Ignition delay times for autoignition, thermal ignition and NSD assisted ignition and (b) discharge energy for ignition used with different E/N as a function of temperature in a stochiometric NH₃/air mixture.

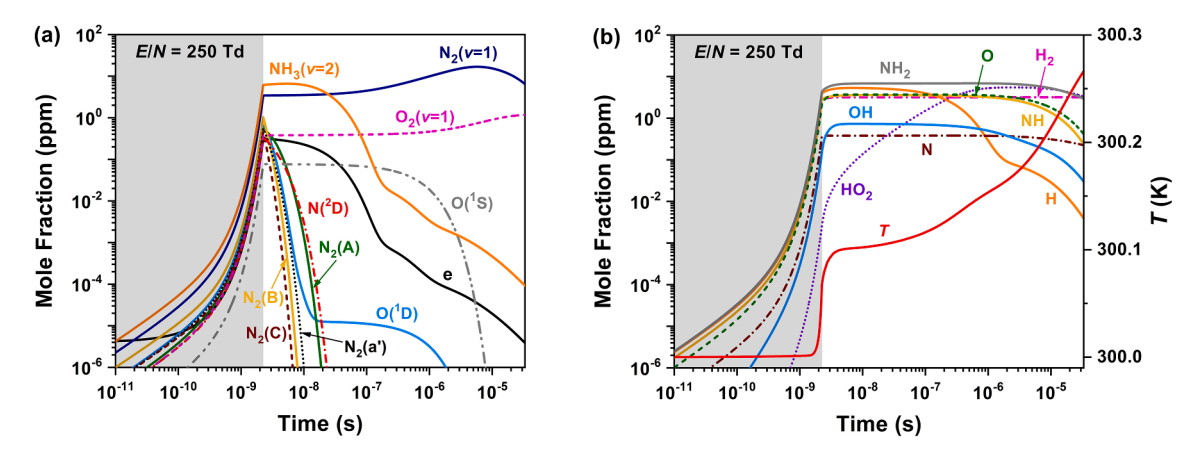


Fig. 4. Time evolutions of (a) excited species and electron as well as (b) radicals and temperature in a single nanosecond discharge pulse at 250 Td and 300 K. (The grey shadow indicates the nanosecond discharge phase).

and (R11). It is noted that the quenching of $O(^1D)$ slows down after 10 ns. This is because $O(^1S)$ also contributes to $O(^1D)$ production by reaction (R12). Correspondingly, a rapid temperature rise is observed during the discharge and early stage of afterglow (<10 ns). This fast gas heating is attributed to the electron impact reactions and quenching of electronically excited species. During the nanosecond discharge, over 80% of fast gas heating is contributed by Franck-Condon (FC) effects due to electron impact dissociation, and the resulting enthalpy change [40,41], as shown in Fig. 5.

$$N_2(A)/N_2(B)/N_2(a') + NH_3 \rightarrow N_2 + NH_2 + H$$
 (R6)

$$N_2(a')/N_2(C) + NH_3 \rightarrow N_2 + NH + H_2$$
 (R7)

$$N_2(B) + O_2 \rightarrow N_2 + O + O$$
 (R8)

$$N_2(a')/N_2(C) + O_2 \rightarrow N_2 + O + O(^1D)$$
 (R9)

$$O(^{1}D) + NH_{3} \rightarrow NH_{2} + OH \tag{R10}$$

$$N(^{2}D) + NH_{3} \rightarrow NH_{2} + NH$$
 (R11)

$$O(^{1}S) + O_{2} \rightarrow O(^{1}D) + O_{2}$$
 (R12)

Fig. 4(b) shows that the radicals are produced during the discharge and afterglow. With the radical consumption and VT relaxation of vibrationally excited species, the temperature increases in the later stage of afterglow (100 ns-10 μ s). To understand the effects of plasma discharge on radical production and therefore low temperature NH₃ oxidation, the path flux analyses of major radicals are conducted, as shown in Fig. 6. To exclude the high temperature NH₃ combustion

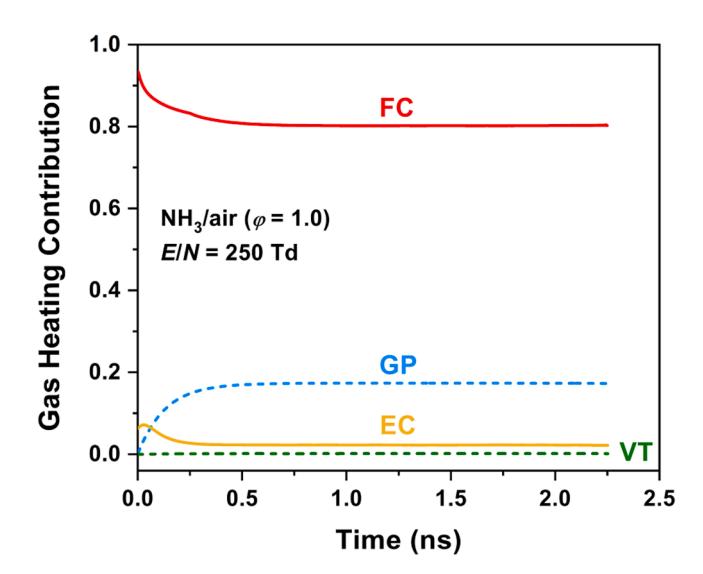


Fig. 5. Gas heating contribution by Franck-Condon effects (FC), vibrational-translational relaxation of vibrationally excited species (VT), gas phase thermochemistry (GP), as well as elastic collisions and ion/neutral charge exchange (EC) in a single nanosecond discharge pulse at 250 Td and 300 K.

chemistry (>1000 K), the path flux is conducted by time integration in the first 1000 discharge pulses. The temperature rises from 300 to 943 K. The results show that 30.5% of NH $_2$ and 94.5% of NH are contributed by

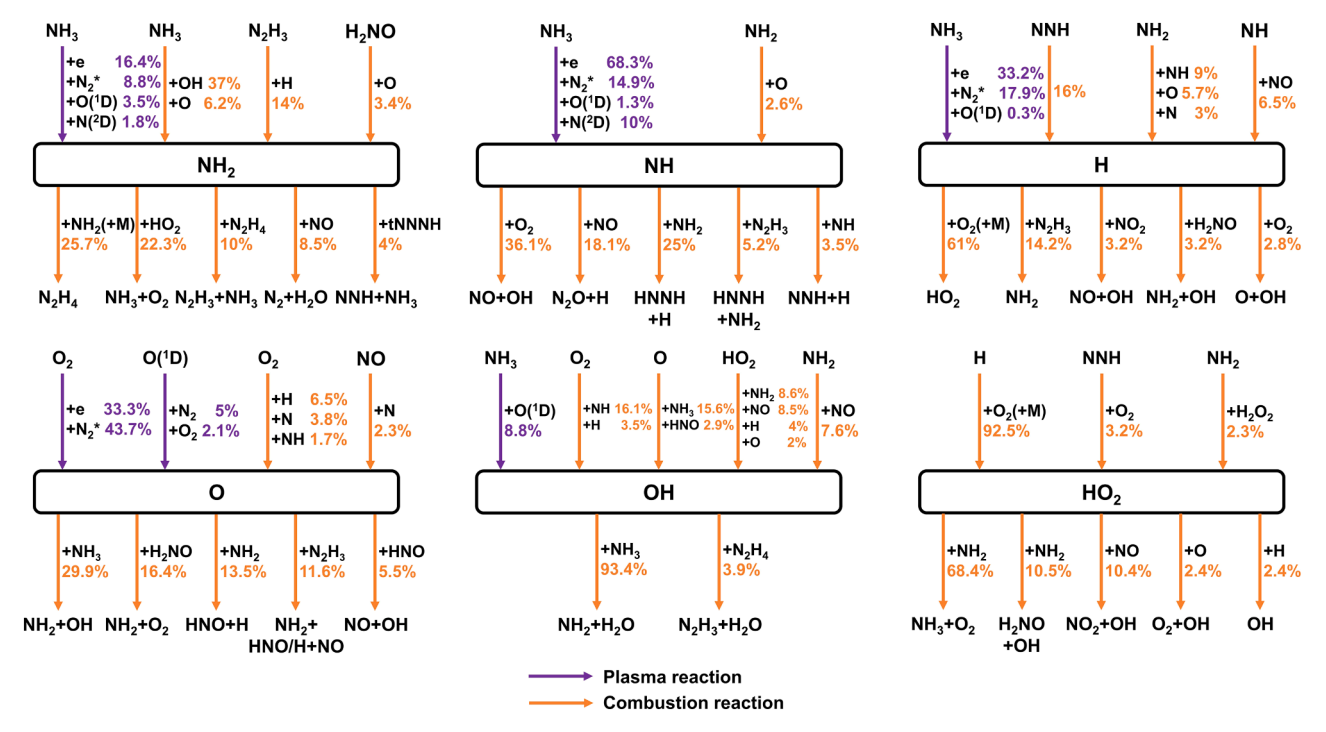


Fig. 6. Path flux analyses of radicals in the first 1000 discharge pulses at 250 Td and 300 K. The path flux is integrated during the whole period between discharge pulses. All percentages do not exactly sum to 100%, as some reactions add small quantities. The percentages indicate the contributions accounting for the species total production and consumption.

the reactions involving electrons (R13-R14) and electronically excited N_2^* , $O(^1D)$ and $N(^2D)$. At the same time, the dissociation of NH_3 by electrons (R13) and N_2^* (R6) contributes to the H production, accounting for 33.2% and 17.9% of its total production, respectively. H radical further contributes to the HO₂ production via addition reaction with O_2 (R15). However, the reaction (R16) between HO_2 and NH_2 is the primary reaction that inhibits NH_3 oxidation at low temperatures, accounting for 22.3% of NH_2 and 68.4% of HO_2 consumption, respectively. For O radical, electrons and N_2^* contribute to 33.3% and 43.7% of O production through reactions (R17-R18) and (R8-R9). Fig. 6 shows that 37% of NH_2 is produced by the reaction (R19) between NH_3 and OH. OH is contributed by the reactions of $O(^1D)$ (R10) as well as radicals NH_2 , NH, H, O and HO_2 generated by plasma. Therefore, it can be concluded that radical production is highly dependent on plasma discharge at low temperatures. The radicals and temperature produced

in discharge bursts accelerate the NH_3 oxidation until the branched-chain thermal explosion and ignition development.

$$e + NH_3 \rightarrow e + NH_2 + H \tag{R13}$$

$$e + NH_3 \rightarrow e + NH + H_2 \tag{R14}$$

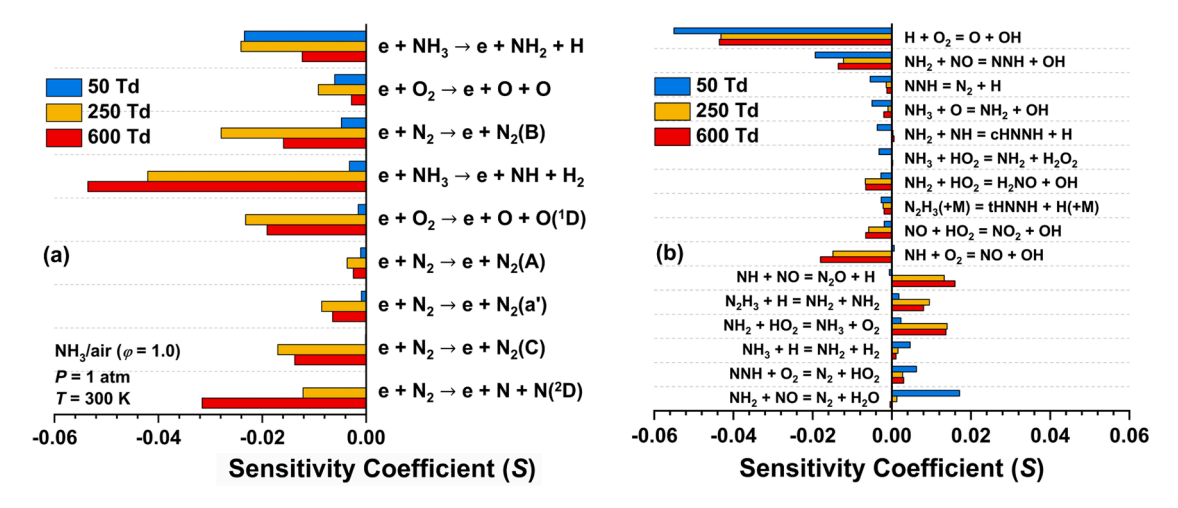
$$H + O_2(+M) = HO_2(+M)$$
 (R15)

$$NH_2 + HO_2 = NH_3 + O_2$$
 (R16)

$$e + O_2 \rightarrow e + O + O \tag{R17}$$

$$e + O_2 \rightarrow e + O + O(^1D)$$
 (R18)

(R19)



 $NH_3 + OH = NH_2 + H_2O$

Fig. 7. Sensitivity coefficients of ignition delay time for (a) electron impact reactions and (b) combustion reactions with different reduced electric field strengthens at 300 K.

sensitivity analysis for ignition delay time is conducted. The normalized sensitivity coefficient of ignition delay time *S* is defined as $(\tau(2k_i) - \tau(k_i))$ / $\tau(k_i)$, where τ represents the ignition delay time and k_i is the rate constant of the jth reaction. The negative sensitivity coefficient represents a promotive effect of the reaction on ignition enhancement and vice versa. Fig. 7(a) shows the sensitivity of ignition delay time for electron impact reactions with different E/N. The results show that the electron impact dissociation reaction of NH₃ (R13) has a large negative sensitivity coefficient at 50 Td, indicating the dominant role in enhancing ignition. All the other electron impact electronic excitation and dissociation reactions have small sensitivities. As shown in Fig. 2, when the E/N is at 50 Td, \sim 4% of discharge energy is deposited into (R13). Over 80% of discharge energy goes the vibrational excitation of $N_2(\nu)$. With the increase of E/N, Fig. 7(a) shows that the dominant electron impact reactions for ignition enhancement become the dissociation of NH3 (R13-R14) and O2 (R17-R18) as well as the electronic excitation of N2 (R20). These channels efficiently accelerate radical production and further enhance ignition at low temperatures. It is noted that the sensitivity of the dissociation reaction of N₂ (R21) increases at 600 Td due to the production of N and N(²D), indicating the role of N (2 D) on NH₃ dissociation at high E/N via (R11).

$$e + N_2 \rightarrow e + N_2*(N_2(A)/N_2(B)/N_2(a')/N_2(C))$$
 (R20)

$$e + N_2 \rightarrow e + N + N(^2D)$$
 (R21)

Fig. 7(b) shows the sensitivity coefficients of combustion reactions. Compared with the sensitivity coefficients of electron impact reactions in Fig. 7(a), the chain-branching reaction (R22) has the largest negative sensitivity coefficient at 50 Td. The ignition is highly dependent on O and OH production. This is because the major species $N_2(\nu)$ produced at 50 Td (see Fig. 2) only provide thermal contribution which are less efficient in enhancing ignition compared with the kinetic enhancement through electronically excited species and radicals. Due to the production of NH₂ by (R13), reaction (R23) also shows promotive effects whereas the consumption by (R24) shows inhibitive effects on ignition enhancement. The production of NNH further enhances ignition by dissociation reaction (R25) with H generation.

$$H + O_2 = O + OH \tag{R22}$$

$$NH_2 + NO = NNH + OH (R23)$$

$$NH_2 + NO = N_2 + H_2O$$
 (R24)

$$NNH = N_2 + H \tag{R25}$$

The results show that at 250 and 600 Td, reactions (R26-R28) enhance ignition due to more NH, NH $_2$ and HO $_2$ production with the increase of E/N. All these reactions contribute to OH production, indicating its importance in enhancing NH $_3$ ignition. The consumption pathways (R16) and (R29) of these radicals are the dominant reactions inhibiting ignition. Note that as one of the NH $_2$ production pathways during ignition, reaction (R30) has a large positive sensitivity coefficient. This is because there exists a competition of N $_2$ H $_3$ consumption between reactions (R30) and (R31). The production of tHNNH by (R31) contributes to the NNH production via reactions with NH $_2$ (R32) and H (R33) and further enhances ignition.

$$NH + O_2 = NO + OH \tag{R26}$$

$$NH_2 + HO_2 = H_2NO + OH$$
 (R27)

$$NO + HO_2 = NO_2 + OH \tag{R28}$$

$$NH + NO = N_2O + H \tag{R29}$$

$$N_2H_3 + H = NH_2 + NH_2 \tag{R30}$$

$$N_2H_3(+M) = tHNNH + H(+M)$$
 (R31)

$$tHNNH + NH_2 = NNH + NH_3 \tag{R32}$$

$$tHNNH + H = NNH + H_2 \tag{R33}$$

Compared with plasma assisted ignition at 50 Td with longer ignition delay time, the results show that more reaction pathways on ignition enhancement are induced due to efficient radical production with the increase of E/N. Therefore, we can conclude that the radicals produced by electron impact dissociation and quenching of electronically excited species (N₂(A), N₂(B), N₂(a'), N₂(C), O(1 D) and N(2 D)) are more effective in ignition enhancement than the vibrationally excited species in NH₃ ignition.

3.3. Effects of equivalence ratio and NO_x formation on ignition enhancement

To reduce NO_x emission, fuel-rich condition is usually applied for NH_3 combustion due to the DeNO_x mechanism [42]. With the plasma discharge, the electron energy distribution function (EEDF) changes with the mixture composition as well as corresponding the plasma-enhanced pathways. In this section, the effects of equivalence ratio and NO_x formation by NSD on ignition enhancement are therefore studied.

Fig. 8 shows the ignition delay time as a function of E/N with different equivalence ratios ($\varphi=0.5, 1.0, \text{ and } 2.0$) at 300 K. It is clear to see that the ignition delay time is non-monotonically dependent on E/N. The maximum ignition enhancement is achieved at E/N=250 Td for all equivalence ratios. It is interesting to note that the ignition enhancement by NSD is more effective at fuel-lean condition with $\varphi=0.5$. This is opposite to the autoignition which the shortest ignition delay time is achieved in a fuel-rich mixture ($\varphi=2.0$) [34]. This is attributed to the efficient production of O, O(1 D) and NO at fuel-lean conditions, which will be discussed in the following.

To understand the plasma enhanced pathways at different equivalence ratios, the sensitivity analysis of ignition delay time is conducted at 250 Td and 300 K, as shown in Fig. 9. Fig. 9(a) shows that reactions (R13) and (R14) have the largest negative sensitivity coefficients at $\varphi=2.0$. This indicates the dominant role of electron impact NH₃ dissociation in enhancing ignition. However, with the decrease of equivalence ratio, the major reactions for ignition enhancement become reactions (R34) and (R18). N₂(B), O(1 D) and O are the dominant species produced by plasma discharge in enhancing ignition. Fig. 10 shows the path flux analyses of N₂(B) and O(1 D) during ignition. The path flux is integrated between the starting point and ignition delay time. From the

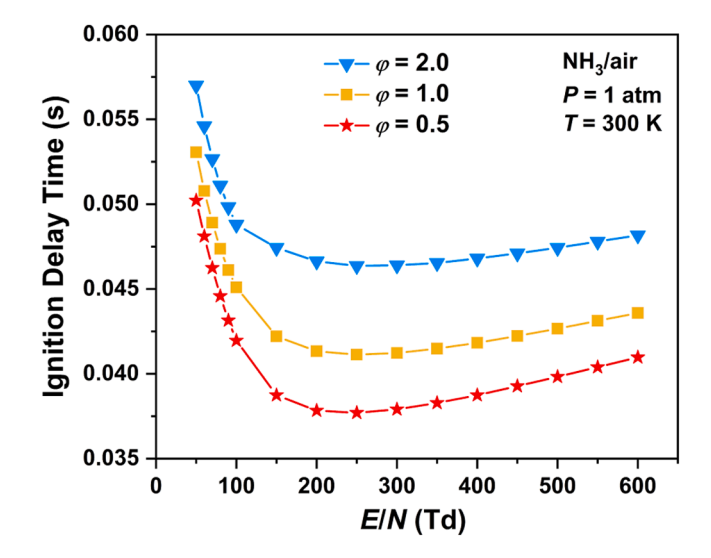


Fig. 8. Ignition delay times with different equivalence ratios as function of E/N at 300 K.

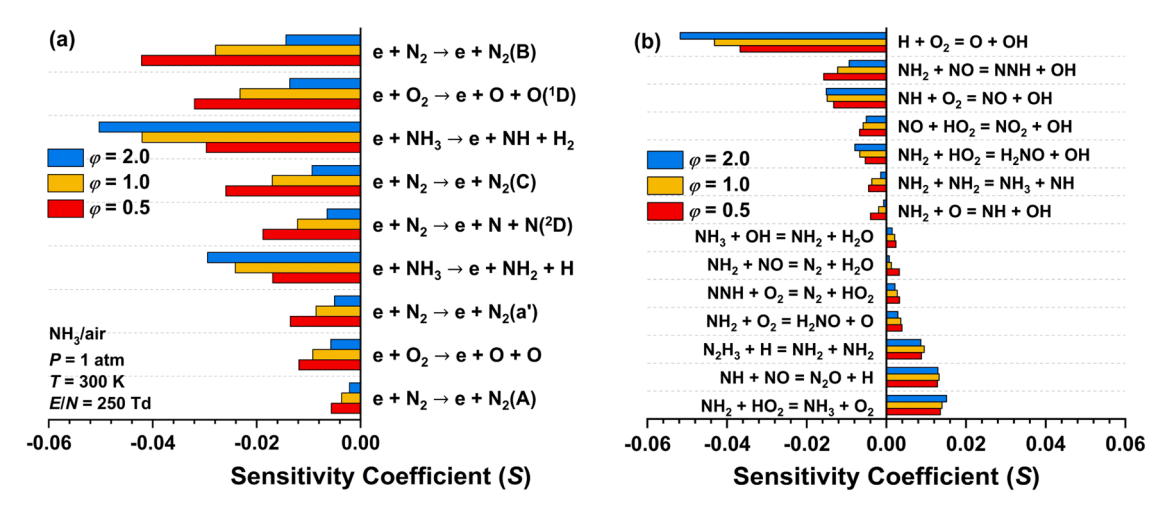


Fig. 9. Sensitivity coefficients of ignition delay time for (a) electron impact reactions and (b) combustion reactions with different equivalence ratios at 250 Td and 300 K.

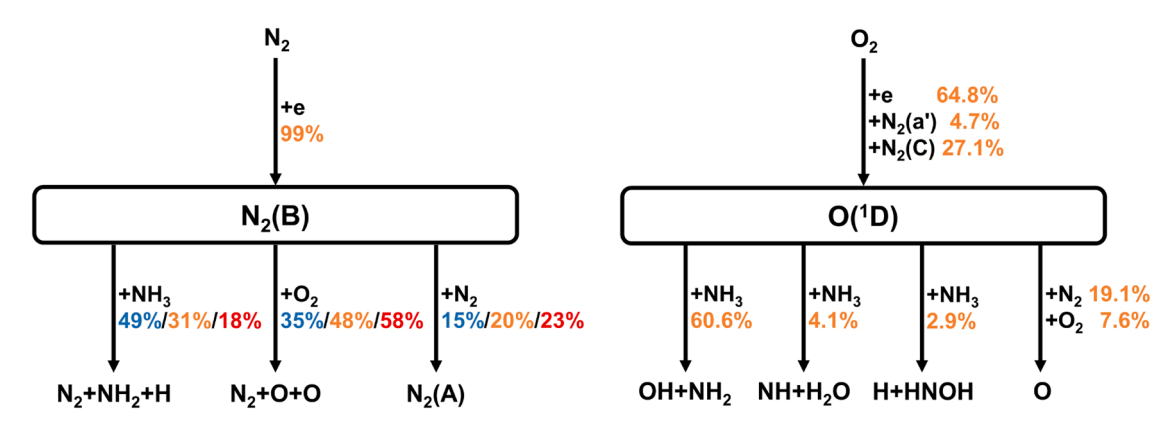


Fig. 10. Path flux analyses of $N_2(B)$ and $O(^1D)$ during ignition in a NH_3 /air mixture at 250 Td and 300 K. The path flux is integrated during the whole period between discharge pulses. All percentages do not exactly sum to 100%, as some reactions add small quantities. The percentages indicate the contributions accounting for the species total production and consumption. (Blue: $\varphi = 2.0$; Orange: $\varphi = 1.0$; Red: $\varphi = 0.5$).

consumption pathways of $N_2(B)$, the results show that reaction (R8) becomes the major consumption pathway contributing to O production with the decrease of equivalence ratio. $O(^1D)$ is mainly consumed by (R10) and promotes the production of OH and NH_2 . The quenching of O (1D) by N_2 (R35) also contributes to the production of O radical. O radical accelerates the NH_3 oxidation and enhances ignition through pathways such as (R36) and (R37). Therefore, with higher percentages of O_2 and N_2 at fuel-lean condition, the efficient production of O and O (1D) significantly enhances ignition. The reactions involving O and O (1D) production are more effective in ignition enhancement compared to the fuel dissociation reactions via electrons. This also explains the reason why the maximum ignition enhancement achieved at 250 Td.

$$e + N_2 \rightarrow e + N_2(B)$$
 (R34)

$$O(^{1}D) + N_{2} \rightarrow O + N_{2}$$
 (R35)

$$NH_3 + O = NH_2 + OH \tag{R36}$$

$$NH_2 + O = NH + OH \tag{R37}$$

Fig. 9(b) shows that the reactions related to NO have larger sensitivities. As shown in Fig. 11(a), the NO mole fraction dramatically

increases with the decrease of equivalence ratio. Due to high NO formation at $\varphi=0.5$, reactions (R23) and (R28) show larger negative sensitivities. The production of NO accelerates the production of NNH and OH and therefore ignition. Due to the efficient production of NH₂ and NH, Fig. 11(a) shows that the NO concentration dramatically decreases at $\varphi=2.0$ by DeNO_x pathways (R23), (R24) and (R29). However, reactions (R24) and (R29) both show prohibitive effects on ignition enhancement. Therefore, the production of NO at fuel-lean condition can also enhance low temperature NH₃ ignition, leading to the maximum ignition enhancement. As a potent greenhouse gas [43], the time evolution of N₂O is shown in Fig. 11(b). Due to the efficient production of NH and NH₂ by plasma, the N₂O concentration increases by reactions (R29) and (R38) at low temperatures, which was discussed in [22]. When the ignition occurs, N₂O is quickly consumed by H radicals via reaction (R39) and decomposes via reaction (R40).

$$NH_2 + NO_2 = N_2O + H_2O$$
 (R38)

$$N_2O + H = N_2 + OH$$
 (R39)

$$N_2O(+M) = N_2 + O(+M)$$
 (R40)

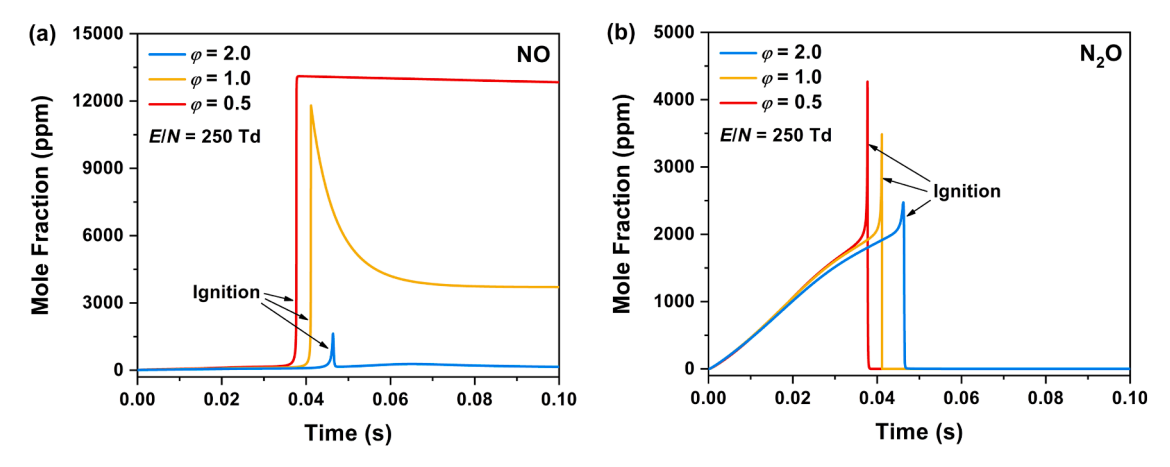


Fig. 11. (a) NO and (b) N_2O formation during plasma assisted ignition with different equivalence ratios at 250 Td and 300 K.

4. Conclusions

The effects of non-equilibrium excitation and NO_x formation in a repetitively-pulsed nanosecond discharge on low temperature NH_3 ignition are studied in this work. An experimentally validated plasma-combustion kinetic model is applied to investigate plasma assisted NH_3 /air ignition at different reduced electric field strengths and equivalence ratios at 300 K and atmospheric pressure.

The results show plasma enhances low temperature ignition and shortens ignition delay time due to the kinetic enhancement via efficient production of excited species and radicals. Ignition fails at the thermal ignition case even significant amount of thermal energy is applied. At low temperatures, the radical production is highly dependent on electron impact dissociation and quenching of electronically excited N2*, O (¹D) and N(²D). This accelerates the OH production and further NH₃ oxidation via $NH_3 + OH = NH_2 + H_2O$. It is found that the ignition delay time is non-monotonically dependent on E/N. There exists an optimum E/N (250 Td) to achieve the maximum ignition enhancement at different equivalence ratios. Vibrationally excited species $NH_3(\nu)$, $O_2(\nu)$ and $N_2(\nu)$ at low E/N are less effective in enhancing ignition, which only induce thermal effects via VT relaxation by NH3 and H2O. Due to efficient radical production with the increase of E/N, more reaction pathways on ignition enhancement are induced. The results show that reactions related to OH production, such as $H + O_2 = O + OH$, $NH_2 + NO = NNH$ + OH and NH + O₂ = NO + OH, show large sensitivities in enhancing low temperature NH_3 ignition. The reactions $NH + NO = N_2O + H$ and $NH_2 + HO_2 = NH_3 + O_2$ show inhibitive effects on ignition.

The plasma assisted ignition at different equivalence ratios also shows that the ignition enhancement is more effective at fuel-lean condition which is opposite to the autoignition case in fuel-rich mixture. The ignition enhancement at fuel-lean condition is attributed to the efficient production of $N_2(B)$, $O(^1D)$ and O. The results show $N_2(B)$ contributes to O production. $O(^1D)$ and O accelerate NH_3 oxidation and enhance ignition through $O(^1D)+NH_3\to NH_2+OH$, $NH_3+O=NH_2+OH$ and $NH_2+O=NH+OH$. These pathways are more effective in ignition enhancement compared with the electron impact dissociation reactions on NH_3 . The results also show that the high concentration of NO at the fuel-lean condition accelerates the production of NNH and OH, leading to the maximum ignition enhancement.

Novelty and significance

The efficient combustion of ammonia (NH_3) offers a promising solution for carbon-neutral future. However, this solution is challenged by high autoignition temperature and NO_x emissions. Non-equilibrium plasma provides a new method for the application of NH_3 in combustion. To understand the kinetic enhanced pathways and the optimized

plasma operating conditions, this work studies plasma assisted low temperature NH_3 /air ignition and NO_x formation by an experimentally-validated plasma-combustion kinetic model. The roles of vibrationally and electronically excited species, radicals, and NO_x formation on NH_3 ignition are discussed. Specifically, there exists an optimal electric field for reducing the ignition delay time. The ignition enhancement by plasma is more effective at fuel-lean conditions due to the faster generation of $N_2(B)$, $O(^1D)$ and O from air. The ignition is also enhanced by NO_x formation in plasma. This work advances the understanding of non-equilibrium excitation and NO_x formation by plasma discharge on low temperature NH_3 ignition.

Author contributions

Xingqian Mao: designed research, performed research, wrote the paper; **Hongtao Zhong:** performed research, wrote the paper; **Ning Liu:** review and editing; **Ziyu Wang:** review and editing; **Yiguang Ju:** designed research, review and editing, supervision.

Declaration of Competing Interest

The authors declare that they have no known competing financial interests or personal relationships that could have appeared to influence the work reported in this paper.

Acknowledgments

This work is supported by the DOE grant DE-SC0020233 of Plasma Science Center and NSF grants CBET 1903362.

Supplementary materials

Supplementary material associated with this article can be found, in the online version, at doi:10.1016/j.combustflame.2023.113140.

References

- A. Valera-Medina, H. Xiao, M. Owen-Jones, W.I. David, P. Bowen, Ammonia for power, Prog. Energy Combust. Sci. 69 (2018) 63–102.
- [2] H. Kobayashi, A. Hayakawa, K.K.A. Somarathne, E.C. Okafor, Science and technology of ammonia combustion, Proc. Combust. Inst. 37 (2019) 109–133.
- [3] C.W. Gross, S.C. Kong, Performance characteristics of a compression-ignition engine using direct-injection ammonia–DME mixtures, Fuel 103 (2013) 1069–1079.
- [4] A. Valera-Medina, R. Marsh, J. Runyon, D. Pugh, P. Beasley, T. Hughes, P. Bowen, Ammonia–methane combustion in tangential swirl burners for gas turbine power generation, Appl. Energy 185 (2017) 1362–1371.
- [5] G. Thomas, Flame acceleration and the development of detonation in fuel—oxygen mixtures at elevated temperatures and pressures, J. Hazard. Mater. 163 (2009) 783–794.

- [6] Y. Ju, W. Sun, Plasma assisted combustion: dynamics and chemistry, Prog. Energy Combust. Sci. 48 (2015) 21–83.
- [7] Y. Ju, J.K. Lefkowitz, C.B. Reuter, S.H. Won, X. Yang, S. Yang, W. Sun, Z. Jiang, Q. Chen, Plasma assisted low temperature combustion, Plasma Chem. Plasma Process. 36 (2016) 85–105.
- [8] A. Starikovskiy, N. Aleksandrov, Plasma-assisted ignition and combustion, Prog. Energy Combust. Sci. 39 (2013) 61–110.
- [9] X. Mao, H. Zhong, T. Zhang, A. Starikovskiy, Y. Ju, Modeling of the effects of non-equilibrium excitation and electrode geometry on H2/air ignition in a nanosecond plasma discharge, Combust. Flame 240 (2022), 112046.
- [10] X. Mao, H. Zhong, Z. Wang, T. Ombrello, Y. Ju, Effects of inter-pulse coupling on nanosecond pulsed high frequency discharge ignition in a flowing mixture, Proc. Combust. Inst. 39 (2023) 5457–5464.
- [11] Y. Bechane, B. Fiorina, Numerical analysis of turbulent flame enhancement by nanosecond repetitively pulsed plasma discharges, Proc. Combust. Inst. 39 (2023) 5465–5476.
- [12] Q. Malé, S. Shcherbanev, N. Noiray, Numerical study of plasma assisted combustion in a sequential combustor, Proc. Combust. Inst. 39 (2023) 5447–5456.
- [13] J. Choe, W. Sun, T. Ombrello, C. Carter, Plasma assisted ammonia combustion: simultaneous NOx reduction and flame enhancement, Combust. Flame 228 (2021) 430–432
- [14] J. Choe, W. Sun, Experimental investigation of non-equilibrium plasma-assisted ammonia flames using NH2* chemiluminescence and OH planar laser-induced fluorescence, Proc. Combust. Inst. (2022).
- [15] Y. Tang, D. Xie, B. Shi, N. Wang, S. Li, Flammability enhancement of swirling ammonia/air combustion using AC powered gliding arc discharges, Fuel 313 (2022), 122674.
- [16] G.T. Kim, J. Park, S.H. Chung, C.S. Yoo, Effects of non-thermal plasma on turbulent premixed flames of ammonia/air in a swirl combustor, Fuel 323 (2022), 124227.
- [17] A. Shioyoke, J. Hayashi, R. Murai, N. Nakatsuka, F. Akamatsu, Numerical investigation on effects of nonequilibrium plasma on laminar burning velocity of ammonia flame, Energy Fuels 32 (2018) 3824–3832.
- [18] G. Faingold, J.K. Lefkowitz, A numerical investigation of NH3/O2/He ignition limits in a non-thermal plasma, Proc. Combust. Inst. 38 (2021) 6661–6669.
- [19] G. Faingold, O. Kalitzky, J.K. Lefkowitz, Plasma reforming for enhanced ammoniaair ignition: a numerical study. Fuel Commun. 12 (2022), 100070.
- [20] T.S. Taneja, P.N. Johnson, S. Yang, Nanosecond pulsed plasma assisted combustion of ammonia-air mixtures: effects on ignition delays and NOx emission, Combust. Flame 245 (2022), 112327.
- [21] M. Shahsavari, A.A. Konnov, A. Valera-Medina, M. Jangi, On nanosecond plasmaassisted ammonia combustion: effects of pulse and mixture properties, Combust. Flame 245 (2022), 112368.
- [22] H. Zhong, X. Mao, N. Liu, Z. Wang, T. Ombrello, Y. Ju, Understanding non-equilibrium N2O/NOx chemistry in plasma-assisted low-temperature NH3 oxidation, Combust. Flame (2023) in press.
- [23] X. Mao, A. Rousso, Q. Chen, Y. Ju, Numerical modeling of ignition enhancement of CH4/O2/He mixtures using a hybrid repetitive nanosecond and DC discharge, Proc. Combust. Inst. 37 (2019) 5545–5552.

- [24] X. Mao, Q. Chen, A.C. Rousso, T.Y. Chen, Y. Ju, Effects of controlled non-equilibrium excitation on H2/O2/He ignition using a hybrid repetitive nanosecond and DC discharge, Combust. Flame 206 (2019) 522–535.
- [25] X. Mao, Q. Chen, C. Guo, Methane pyrolysis with N2/Ar/He diluents in a repetitively-pulsed nanosecond discharge: kinetics development for plasma assisted combustion and fuel reforming, Energy Convers. Manage. 200 (2019), 112018.
- [26] S. Pancheshnyi, B. Eismann, G.J.M. Hagelaar, L.C. Pitchford, Computer code ZDPlasKin, 2008.
- [27] R.J. Kee, F.M. Rupley, J.A. Miller, Chemkin-II: A Fortran Chemical Kinetics Package for the Analysis of Gas-Phase Chemical Kinetics, Sandia National Lab. (SNL-CA), Livermore, CA (United States), 1989.
- [28] G. Hagelaar, L.C. Pitchford, Solving the Boltzmann equation to obtain electron transport coefficients and rate coefficients for fluid models, Plasma Sources Sci. Technol. 14 (2005) 722.
- [29] S. Pancheshnyi, S. Biagi, M. Bordage, G. Hagelaar, W. Morgan, A. Phelps, L. Pitchford, The LXCat project: electron scattering cross sections and swarm parameters for low temperature plasma modeling, Chem. Phys. 398 (2012) 148, 153
- [30] Hayashi database, www.lxcat.net, September 1, 2022.
- [31] Biagi database, www.lxcat.net, September 1, 2022.
- [32] Phelps database, www.lxcat.net, September 1, 2022.
- [33] Morgan database, www.lxcat.net, September 1, 2022.
- [34] L.S. Thorsen, M.S. Jensen, M.S. Pullich, J.M. Christensen, H. Hashemi, P. Glarborg, V.A. Alekseev, E.J. Nilsson, Z. Wang, B. Mei, High pressure oxidation of NH3/n-heptane mixtures, Combust. Flame 254 (2023), 112785.
- [35] H. Zhao, X. Yang, Y. Ju, Kinetic studies of ozone assisted low temperature oxidation of dimethyl ether in a flow reactor using molecular-beam mass spectrometry, Combust. Flame 173 (2016) 187–194.
- [36] A. Rousso, X. Mao, Q. Chen, Y. Ju, Kinetic studies and mechanism development of plasma assisted pentane combustion, Proc. Combust. Inst. 37 (2019) 5595–5603.
- [37] H. Zhong, X. Mao, A.C. Rousso, C.L. Patrick, C. Yan, W. Xu, Q. Chen, G. Wysocki, Y. Ju, Kinetic study of plasma-assisted n-dodecane/O2/N2 pyrolysis and oxidation in a nanosecond-pulsed discharge, Proc. Combust. Inst. 38 (2021) 6521–6531.
- [38] N. Liu, H. Zhong, T.Y. Chen, Y. Lin, Z. Wang, Y. Ju, Sensitive and single-shot OH and temperature measurements by femtosecond cavity-enhanced absorption spectroscopy, Opt. Lett. 47 (2022) 3171–3174.
- [39] N. Liu, T.Y. Chen, H. Zhong, Y. Lin, Z. Wang, Y. Ju, Femtosecond ultraviolet laser absorption spectroscopy for simultaneous measurements of temperature and OH concentration, Appl. Phys. Lett. 120 (2022).
- [40] M.W. Kiehlbauch, D.B. Graves, Temperature resolved modeling of plasma abatement of perfluorinated compounds, J. Appl. Phys. 89 (2001) 2047–2057.
- [41] T. Farouk, B. Farouk, D. Staack, A. Gutsol, A. Fridman, Modeling of direct current micro-plasma discharges in atmospheric pressure hydrogen, Plasma Sources Sci. Technol. 16 (2007) 619.
- [42] M.A. Kimball-Linne, R.K. Hanson, Combustion-driven flow reactor studies of thermal DeNOx reaction kinetics, Combust. Flame 64 (1986) 337–351.
- [43] P. Wolfram, P. Kyle, X. Zhang, S. Gkantonas, S. Smith, Using ammonia as a shipping fuel could disturb the nitrogen cycle, Nature Energy 7 (2022) 1112–1114.